Bulletin of the Seismological Society of America, Vol. 97, No. 3, pp. 961–976, June 2007, doi: 10.1785/0120060156

Liquefaction, Ground Oscillation, and Soil Deformation at the Wildlife Array, California

by Thomas L. Holzer and T. Leslie Youd

Abstract Excess pore-water pressure and liquefaction at the Wildlife Liquefaction Array in 1987 were caused by deformation associated with both high-frequency strong ground motion and 5.5-second-period Love waves. The Love waves produced large (~1.5%) cyclic shear strains well after the stronger high-frequency ground motion abated. These cyclic strains generated approximately from 13 to 35% of the excess pore-water pressure in the liquefied layer and caused excess pore-water pressures ultimately to reach effective overburden stress. The deformation associated with the Love waves explains the "postearthquake" increase of pore-water pressure that was recorded at the array. This explanation suggests that conventional methods for predicting liquefaction based on peak ground acceleration are incomplete and may need to consider cyclic strains associated with long-period surface waves. A postearthquake survey of an inclinometer casing indicated permanent shear strain associated with lateral spreading primarily occurred in the upper part of the liquefied layer. Comparison of cone penetration test soundings conducted after the earthquake with pre-earthquake soundings suggests sleeve friction increased. Natural lateral variability of the liquefied layer obscured changes in tip resistance despite a ~1% reduction in volume. The large oscillatory motion associated with surface waves explains ground oscillation that has been reported at some liquefaction sites during earthquakes.

Introduction

It has been nearly 20 years since the Wildlife Liquefaction Array recorded strong ground motion and pore-water pressure buildup in a sand undergoing liquefaction. Many investigations and analyses of the records have been conducted since our initial report on the field recording of liquefaction (Holzer *et al.*, 1989b). Although some features of the performance of the array have been clarified by these studies, two outstanding questions remain. Was the delayed buildup of pore-water pressure an intrinsic aspect of the liquefaction process? If so, what caused it? Here we propose an answer to these two questions by building on analyses and investigations published during the intervening years. We conclude that: (1) the piezometers measured the true buildup of pore-water pressure in the liquefying sand, and (2) the delay in the buildup was caused by ~10-cm amplitude long-period (~5.5 sec) Love waves that continued to cyclically strain the softened sand layer at Wildlife during the tens of seconds after the primary strong motion had subsided.

In addition, we describe subsurface deformation measured in an inclinometer casing after the earthquake and discuss its implications. The inclinometer provides insight into where shear strains in the liquefied sand were concentrated, which has implications for pipeline and pile design. We also compare cone penetration tests (CPT) conducted before and after the earthquake, which suggest changes in soil density caused by liquefaction if any were modest. The results have implications for the Seed–Idriss simplified procedure (Youd *et al.*, 2001), which is based on postearthquake penetration tests.

We adopt here the definition of "liquefaction" by Seed and Lee (1966). A soil is considered to have liquefied when its resistance to deformation is zero over a wide range of strain amplitude. Under field conditions, this occurs when excess pore-water pressure approaches the effective overburden stress.

Wildlife Liquefaction Array and the 1987 Superstition Hills Earthquake

The Wildlife Liquefaction Array was established in 1982 on the flood plain of the Alamo River in the Imperial Valley desert of southern California (Fig. 1). The site is located where sand boils developed during the 1981 Westmorland earthquake (Youd and Wieczorek, 1982). Although the site is on level ground, the center of the array is only

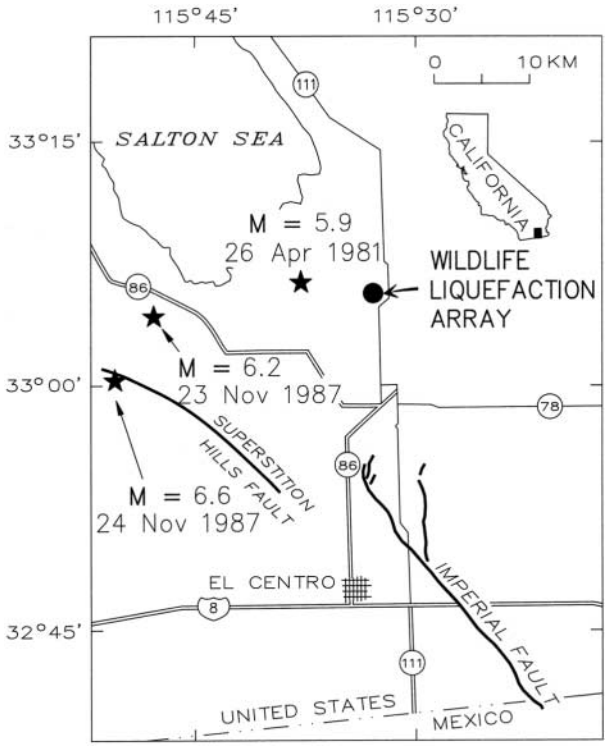

Figure 1. Location map of Imperial Valley (Holzer *et al.*, 1989b). The *M* 6.6, *M* 6.2, and *M* 5.9 earthquakes, respectively, are the Superstition Hills, Elmore Ranch, and Westmorland.

23 m from the west bank of the river, which has cut a 3.7-m-deep channel into the flood plain. The Alamo River, which is sustained by agricultural drainage, flows year round at an approximately constant discharge. This maintains the water table at an approximately constant depth of 1.2 m.

Subsurface conditions and geotechnical properties of sediment at the Wildlife array are described by Bennett *et al.* (1984), Bierschwale (1984), and Vucetic and Dobry (1986) and are summarized in Table 1. The table is based on samples from borings immediately next to the instrumented area. The stratigraphy at the array consists of saturated Holocene floodplain sediments that were deposited in an old incised river channel. The floodplain sediments are about 7 m thick and overlie denser and more regionally extensive sedimentary deposits (Fig. 2). The floodplain sediments consist of a 2.5-m-thick layer of lean clay to silt (CL-ML), which is underlain by the 4.3 m of liquefiable silty sand. The upper 1 m of the liquefiable layer is actually sandy silt (ML) with an average fines content of 78%. The lower 3.3 m is silty sand (SM) with an average fines content of 36%. These two layers will be collectively referred to as either the liquefiable or sand layer. These sediments are geologically young. A wood fragment collected from a depth of 6 m in the floodplain sediments yielded a radiocarbon date of only 230 ± 130 years B.P. (1950), which is a maximum age. The sediment probably was deposited by flood water from the Colorado River that flowed down the Alamo River in 1905–1907.

Sensors at the array consisted of two three-component force-balanced accelerometers and six pore-pressure transducers (Figs. 2 and 3). The accelerometers were placed at the surface and in a cased boring at a depth of 7.5 m. The latter accelerometer will be referred to as the downhole. Five of the pore-pressure transducers were installed in the sand layer at depths ranging from 2.9 to 6.6 m; the sixth was in a dense 1-m-thick silt layer beneath the floodplain sediments at a depth of 12 m. Piezometer P4 had failed by November 1987.

The Wildlife Liquefaction Array triggered four times during the Superstition Hills earthquake sequence of 23–24 November 1987, including a *M* 6.2 foreshock approximately 9 hours before the mainshock. This foreshock was named the Elmore Ranch earthquake. Only the *M* 6.6 mainshock, the Superstition Hills earthquake, liquefied the 4.3-m-thick sand layer (Holzer *et al.*, 1989b). Liquefaction caused water and muddy sediment to erupt and cover much of the land surface after the earthquake. Surface effects were mapped by Holzer *et al.* (1989a) after the earthquake (Fig. 3). Although no water was discharging, water was still standing at the array when it was inspected by the first author at 1530 PST, about 10 hours after the mainshock. The eruption of water and sediment may have lasted for tens of minutes. The most direct evidence for a lengthy eruption period is that pore-water pressures were still elevated during the aftershock that occurred 19 minutes after the mainshock and triggered the array (Holzer *et al.*, 1989b). Indirect evidence includes the stratigraphy and morphology of the sand boils, which must have taken at least several minutes if not tens of minutes to form. Alternating layers of fine- and coarse-grained material in sand boils, as revealed in cross section, presumably developed gradually as discharge fluctuated. In addition, several sand boils had steep outer margins indicative of subaqueous deposition. The margins were revealed after the water level subsided. These boils discharged enough water that they eventually became islands standing in their own effluent while they continued to discharge water and sediment. Comparison of grain-size distributions of sand boils with subsurface samples from borings indicated that material vented from both the upper sandy silt and lower silty sand layers (Bennett, 1988).

Ground cracks accompanied the eruption of sand boils and indicate that permanent ground displacement occurred (Fig. 3). Ejection of sand from the cracks confirms that the cracks were associated with liquefaction. Although most of the cracking was caused by local slumping of the west bank of the Alamo River eastward toward the river, a N63°W-trending 15-m-long crack through the instrumented array indicates permanent ground displacement occurred in the array (Fig. 3). Horizontal extension across this crack was 10 mm in a N27°E direction. Cumulative opening across ground cracks was 126 mm. Resurveys of control points after the earthquake indicate the overall pattern of permanent ground displacement near the array (Youd and Bartlett, 1989). Displacements of the control points are shown in Figure 3. The

Table 1
Geotechnical Properties of Soils near Instrumented Area*

Depth (m)	q_c (MPa)	R_f (%)	D_{50} (mm)	Fines <75 μm (%)	Clay <5 μm (%)	V_s (m/sec)	wc (%)	Atterburg Limits (%) LL	Atterburg Limits (%) PL	USCS Soil Type
0–2.5	0.60 ± 0.36	3.41 ± 4.72	0.025	93 ± 8	25 ± 16	99	32 ± 4.8	30 ± 4.6	22 ± 2.7	CL-ML
2.5–3.5	1.87 ± 1.00	0.87 ± 0.75	0.055	78 ± 6	8 ± 3	116				ML
3.5–6.8	5.68 ± 2.26	1.01 ± 0.67	0.091	36 ± 12	5 ± 3					SM
6.8–12	2.04 ± 1.30	7.14 ± 5.29	0.005	98 ± 2	60 ± 19	168	28 ± 2.2	59 ± 13.4	30 ± 7	CH
12–17.5	9.38 ± 1.69	2.38 ± 0.45	0.027	94 ± 6	18 ± 10		28 ± 3.3	35 ± 10.8	24 ± 2.1	CL, ML, SM

*q_c is tip resistance; R_f is friction ratio; D_{50} is median grain-size diameter; V_s is shear-wave velocity; wc is water content; LL is liquid limit; PL is plastic limit; and USCS is Unified Soil Classification System.

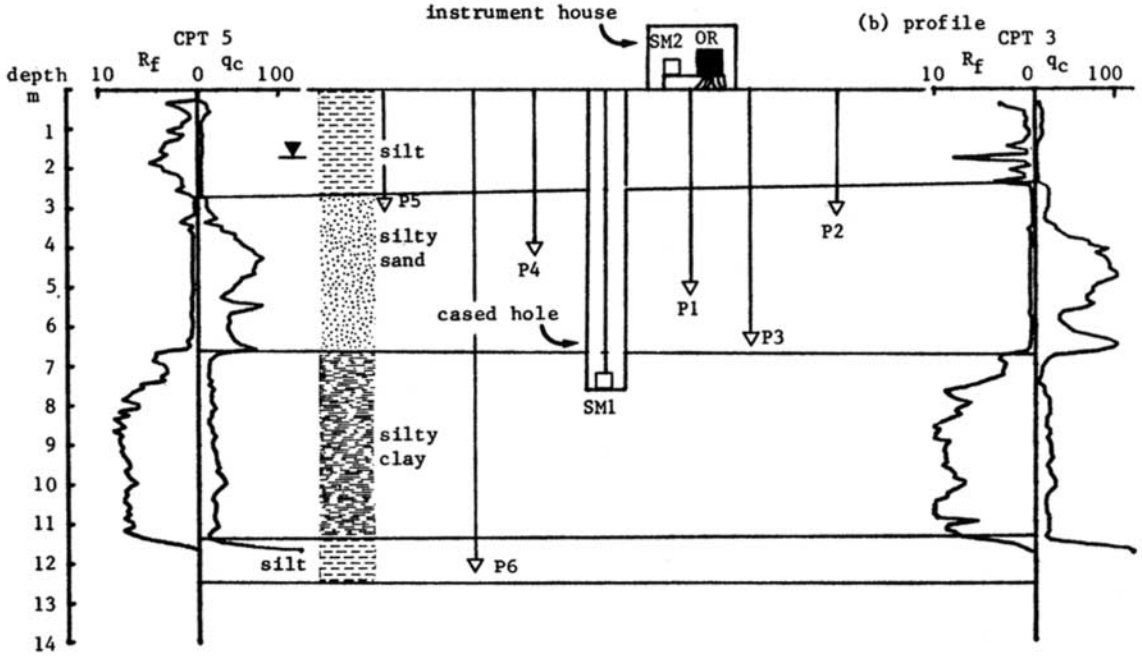

Figure 2. Schematic cross section through Wildlife Liquefaction Array (Bennett *et al.*, 1984).

displacements are relative to a reference point ~30 m west of 5Cg and 6Cg in an area without surface evidence of liquefaction. Displacements of 107 mm were measured just east of the array in N25°E and N39°E directions, respectively, at control points at 2Cg and 3Cg. No displacement was detected at control points at 5Cg and 6Cg just west of the array.

Recordings of the 1987 Superstition Hills Earthquake

Strong-motion and pore-water pressure measurements from the *M* 6.6 Superstition Hills earthquake are shown in Figures 4 and 5. Only the two horizontal components of acceleration from both the downhole and surface accelerographs are shown along with the record from piezometer P5. Complete records from the array were published by Holzer *et al.* (1989b) and are available at http://nsmp.wr.usgs.gov; they are not essential to illustrate the interpretation that will be developed here. Only the pore-water pressure recording from P5, which was buried in the top of the sandy silt layer, is shown here because the performance of the other piezometers was disputed (Earth Technology Corporation, 1991; Hushmand *et al.*, 1991, 1992; Scott and Hushmand, 1995). The performance of P5, however, was not challenged. This issue will be revisited in the *Discussion*. The peak ground acceleration (PGA), -202 cm/sec^2, was recorded on the north–south accelerometer at 13.6 sec. The corresponding downhole PGA was -171 cm/sec^2.

Excess pore-water pressure started to develop at 13.6 sec at P5. The onset is coincident with the peak horizontal acceleration in both the surface and downhole accelerograms. Pore-water pressure unexpectedly increased slowly, but at a decreasing rate, until the end of the 97-sec-long record well after the strongest motion had subsided. Thirteen percent of the excess pore-water pressure at P5 developed after 90% of the earthquake shaking had propagated through the site (36.4 sec after triggering) as measured by

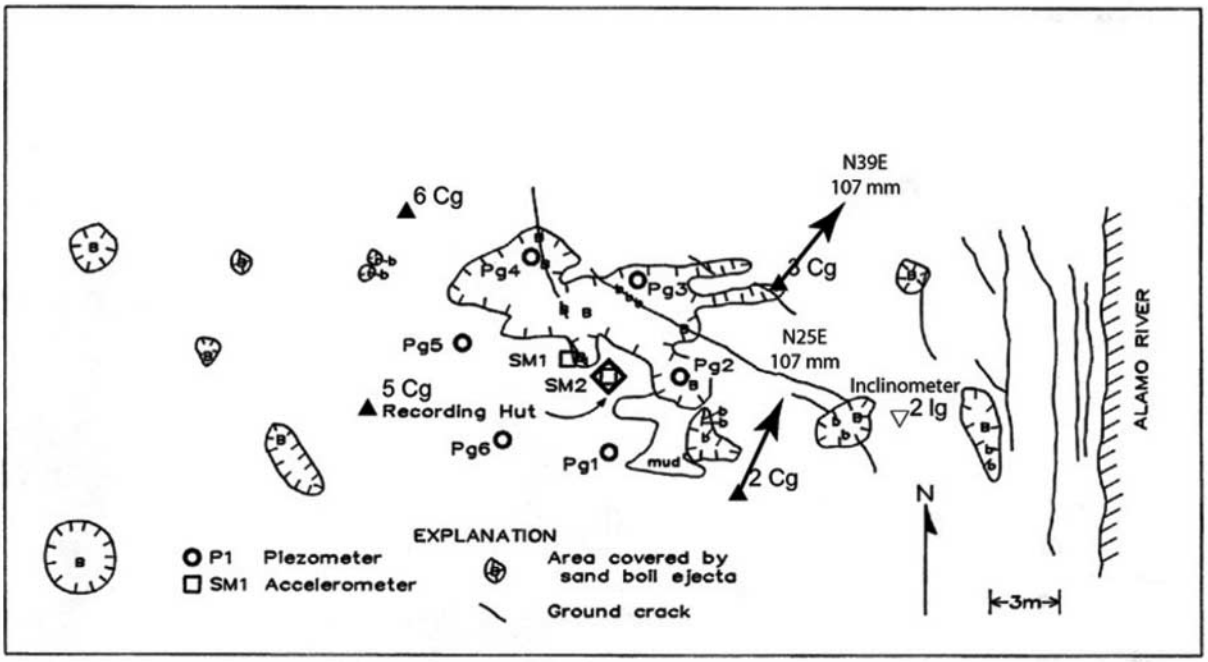

Figure 3. Map of liquefaction effects caused by 24 November 1987, Superstition Hills earthquake, instrumentation, and CPT soundings (modified from Holzer *et al.*, 1989a). Piezometers are labeled as Pg and CPT soundings as Cg. Displacements of control points are from Youd and Bartlett (1989). No displacements were measured at 5Cg and 6Cg.

the accumulated Arias (1969) Intensity in the two downhole horizontal accelerometers.

Two adjustments—for drift and calibration—were made to the pore-water pressure record of P5 shown in Figures 4 and 5. The original recording suggests approximately 3 kPa ($r_U = 0.06$) of excess pore-water pressure developed before 13.6 sec. However, the small transducer signal for the first 13.6 sec is identical with the signal recorded during the *M* 6.2 foreshock as well as two smaller shocks that triggered the recording system. The signal increased slowly for about 30 sec, when the transducer output stabilized, in these other three events. We assume the small increase was instrumental drift that was associated with warm-up of the pore-water pressure transducer, which was not powered until the recording system triggered. To remove the drift from P5, the signal recorded during the *M* 6.2 foreshock, which also was digitized, was subtracted from the mainshock recording. Without this correction, the implied small amount of pore-pressure increase at the beginning of the record when ground motion was small would require an explanation. Liquefaction is not predicted for the Elmore Ranch earthquake by the Seed-Idriss simplified procedure (Holzer *et al.*, 1989b) (Fig. 6). The second adjustment was to compensate for uncertainty in the calibration of the transducer. As was noted by Holzer *et al.* (1989b) (Fig. 3), the pore-water pressure at P5 slightly exceeded the effective overburden stress if one accepts the calibration of the transducer. Because we do not have sufficient confidence in the calibration to believe this unexpected measurement, we plot the pore-water pressure as the excess pore-water pressure ratio by assuming the pore-water pressure at 97 sec equaled the effective overburden stress.

The Wildlife pore-water pressure and acceleration time histories were recorded on film, and then scanned and digitally sampled at 50 and 200 samples per second, respectively. Additional processing was applied to each of the acceleration time histories by first making a baseline correction by subtracting the mean of the record, and then filtering to suppress or remove noise at both low and high frequencies. Removing low-frequency noise, which can be caused by digitizing, instrumental drift, and tilting of an accelerometer, is particularly important when the acceleration time histories are doubly integrated to obtain displacement time histories. Otherwise, calculated displacements can be unrealistically large and overwhelm the actual displacements. Low frequencies were removed from the Wildlife accelerograms using an acausal (zero-phase shift) filter in the form of a fourth-order Butterworth filter with a corner frequency at 0.08 Hz that was passed bidirectionally (forward and backward in time) to the time series. In addition, a high-cut filter in the form of a cosine taper between 40 and 50 Hz was applied in the spectral domain to remove high-frequency noise. The practical significance of the filtering is that the resulting signals are band limited in frequency, so that features that are characterized predominantly by long periods, such as permanent displacements, are not well preserved or are lost.

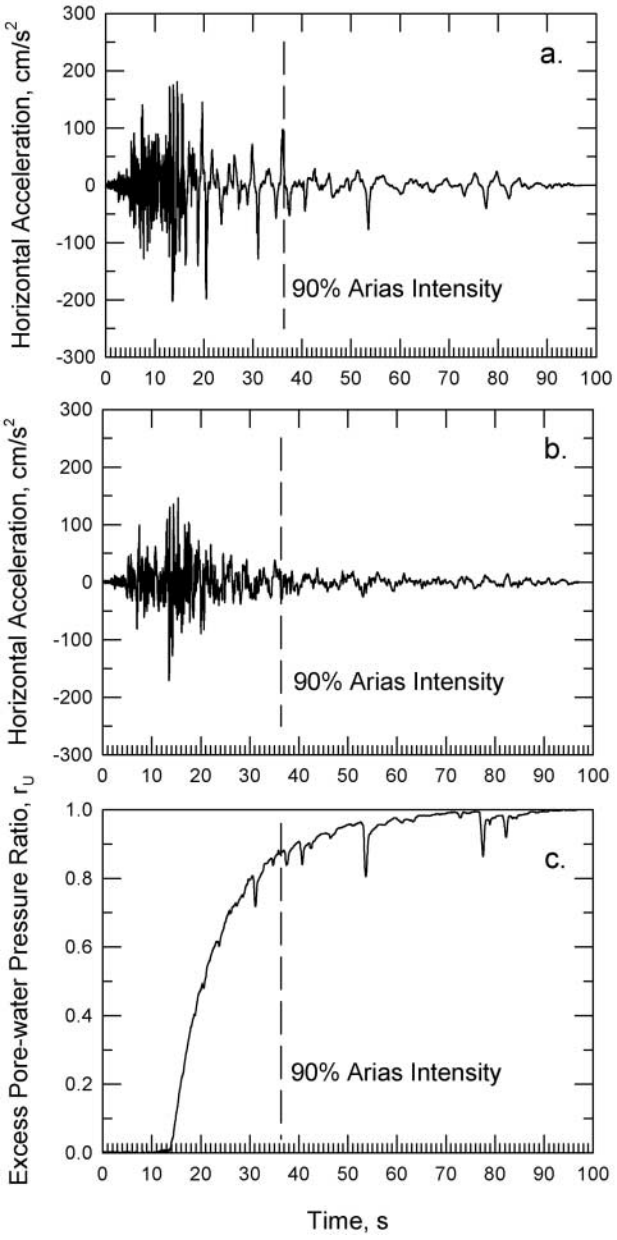

Figure 4. Time histories of north–south surface accelerations (a), north–south downhole accelerations (b), and excess pore-water pressure ratio recorded by piezometer P5 (c). Ratio was computed by dividing recorded value by value at 97 sec.

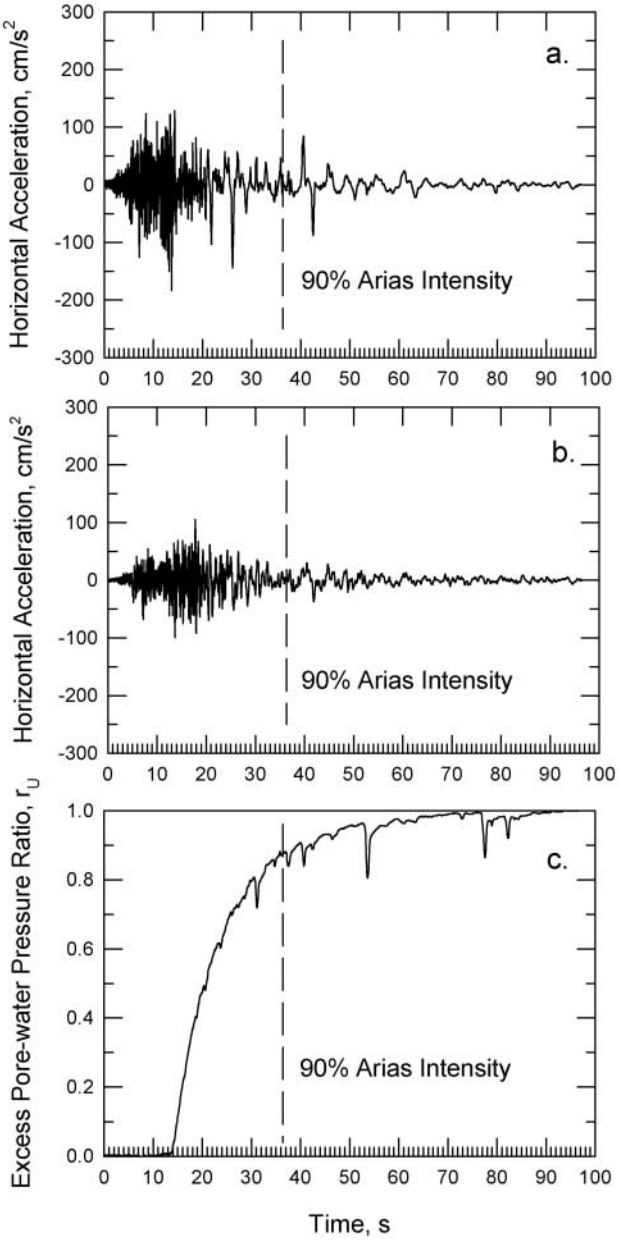

Figure 5. Time histories of east–west surface accelerations (a), east–west downhole accelerations (b), and excess pore-water pressure ratio recorded by piezometer P5 (c).

Summary of Previous Work

Many significant and insightful investigations of the Wildlife recordings have been conducted (Hushmand *et al.*, 1992; Gu *et al.*, 1994; Zeghal and Elgamal, 1994; Glaser, 1996; Davis and Berrill, 2000; Bonilla *et al.*, 2005; Youd and Carter, 2005). The most relevant of these to the present investigation is Zegahl and Elgamal (1994).

Zeghal and Elgamal (1994) were the first to demonstrate that the buildup of pore-water pressure at Wildlife at low levels of shaking was accompanied by strain softening. They calculated time histories of transient shear stress and average seismic strain from the recordings of the horizontal accelerometers. Horizontal shear stress at depth z was estimated from equation (1). Average seismic shear strain from the surface to a depth of 7.5 m was estimated with equation (2).

$$\tau_Z = \frac{1}{2}\rho z(a_S + a_Z) \tag{1}$$

$$\gamma = \frac{d_{DH} - d_S}{7.5} \tag{2}$$

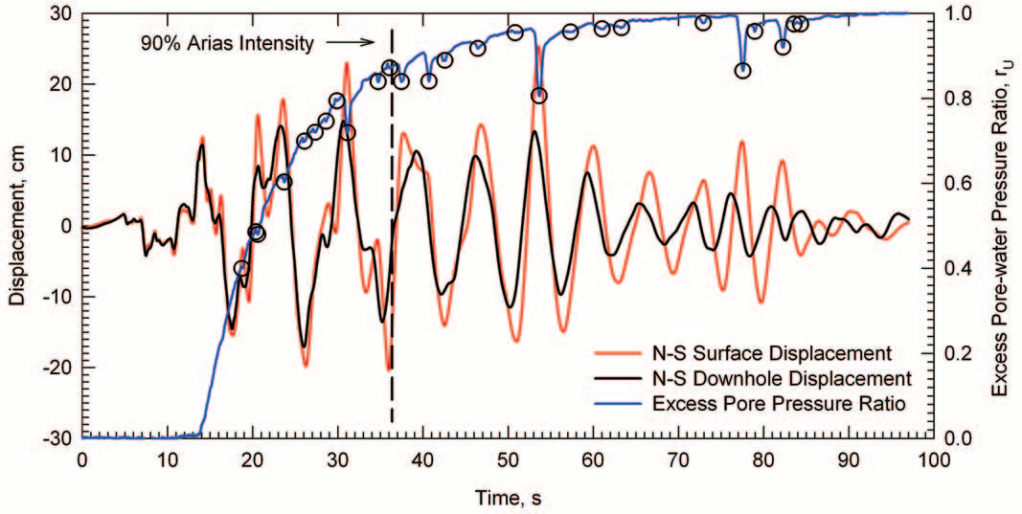

Figure 6. Time histories of north–south displacements computed from surface and downhole accelerograms and excess pore-water pressure ratio recorded by P5. Drops in pore-water pressure are circled.

where a_S = horizontal acceleration recorded at the surface; a_Z = horizontal acceleration at depth z evaluated by linear interpolation using $a_Z = a_S + (a_{DH} - a_S)(z/7.5)$, where a_{DH} = horizontal acceleration recorded by the downhole accelerometer at 7.5 m; γ is the average seismic shear strain between the land surface and 7.5 m; and d_{DH} and d_S, respectively, are the horizontal displacements obtained by double integration of the acceleration histories of the downhole and surface accelerometers. They assumed a soil density, ρ, of 2000 kg/m^3.

They concluded that as the pore-water pressure increased, soil stiffness gradually decreased. After the excess pore-water pressure increased to approximately 50% of the effective overburden stress, transient or dynamic deformation of the upper 7.5 m of soil at Wildlife was characterized by cycles of large shear strain at small shear stress. We have reproduced their calculations and use them in Figures 6–9 to expand the preceding summary. We have switched d_{DH} and d_S in equation (2) so that northward shear strain is positive. Minor differences between the figures presumably are due to filtering applied by Zegahl and Elgamal (1994). Figure 6 shows the time histories of the north–south displacements at the surface and at 7.5 m depth that were computed from the north–south surface and downhole accelerograms. Comparison of the two displacement time histories indicates that, in general, displacements were larger at the surface than at 7.5 m and underwent a phase shift with time. Zegahl and Elgamal (1994) interpreted this behavior as evidence for strain softening associated with pore-water pressure buildup. Note that the spikelike drops of pore-water pressure measured by P5, at 2.9 m, correlate with reversals in the direction of surface displacement. Zegahl and Elgamal (1994) attributed these spikes to strain hardening (dilatancy) of the liquefying layer.

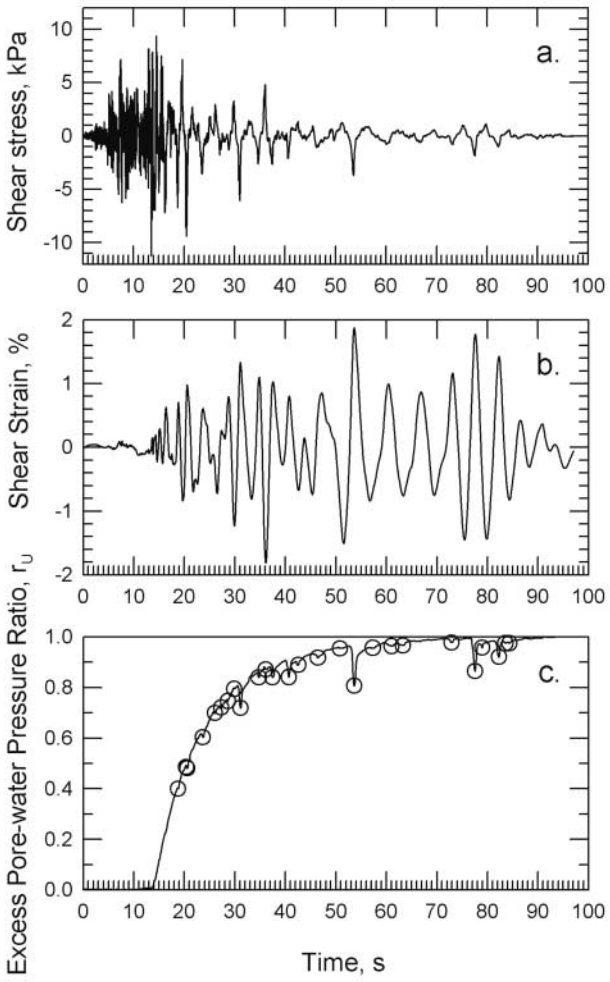

Figure 7. Time histories of north–south shear stress (a), north–south shear strain (b), and excess pore-water pressure ratio in piezometer P5 (c). Pore-water pressure drops at P5 are circled.

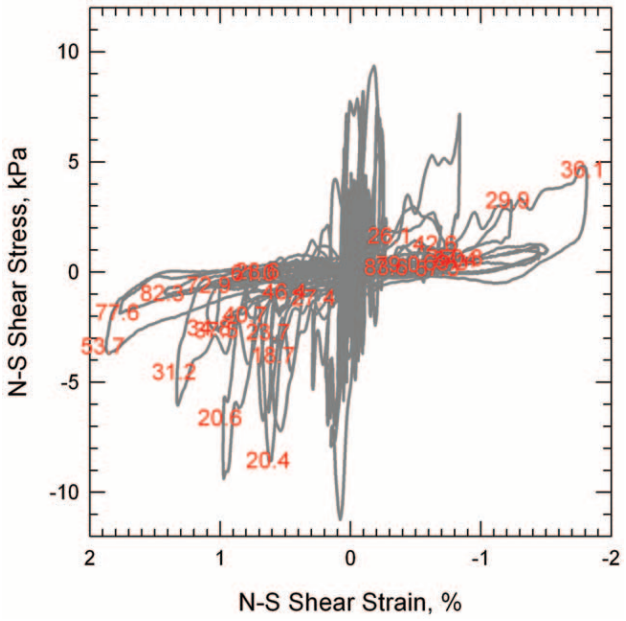

Figure 8. North–south stress-strain history, 0 to 97 sec. Times of pore-water pressure drops recorded by P5 are labeled in red on hysteresis curves. Decimal point shows approximate location on hysteresis curve of pressure drop.

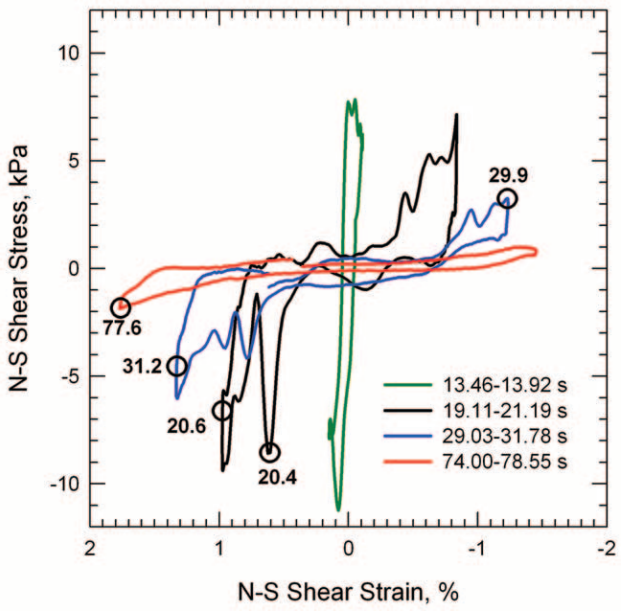

Figure 9. North–south hysteresis curves for four time periods. Curves were selected from Figure 8. Times of pore-water pressure drops recorded by P5 are labeled on hysteresis curves.

Figure 7 compares the time histories of north–south shear stress at 2.9 m with the average shear strain computed with equation (2) based on the displacements shown in Figure 6. Large shear strains persisted with time despite decreasing dynamic shear stress. The spikes in the shear stress history corresponded to the episodes of dilatancy and strain hardening as indicated by the pore-water pressure drops. The softening of the liquefying layer can be documented by plotting shear stress versus average seismic shear strain (Fig. 8). The strain axis in Figure 8 is reversed so the graph can be compared directly to that published by Zegahl and Elgamal (1994) (Fig. 9). The changing slope of the resulting hysteresis curves with time indicates that the shear modulus of the soil was decreasing, that is, the soil was softening. Zegahl and Elgamal (1994) identified only 13 pore-water pressure drops in their investigation. Amplification of the pore-water pressure record shown in Figure 7, however, enabled us to identify at least 13 more drops. The times of these 26 drops are labeled on the hysteresis curves in Figure 8. Pressure drops were associated with most of the episodes of strain hardening.

To illustrate more clearly the softening phenomenon identified by Zegahl and Elgamal (1994), four hysteresis curves were selected from Figure 8. These are shown in Figure 9 with their time intervals as well as the times of pore-water pressure drops in P5. The systematic decrease of the slope of the hysteresis curves with time—the evidence for soil softening—is obvious. In addition, the increase in slope at the end of each hysteresis loop, which is the evidence for strain hardening, is more easily discerned. The association of the drops of pore-water pressure, which suggests dilatant behavior, with the episodes of strain hardening is also clearer.

Seismic Loading

Although Zegahl and Elgamal (1994) convincingly documented strain softening at Wildlife, they did not comment on the nature of the seismic excitation. In other words, they did not explain why the surface continued to experience oscillatory ground motion even after most of the strong ground motion was over. We generated Figure 6 in the process of reproducing the analysis of Zegahl and Elgamal (1994). The striking aspect of Figure 6 from a seismological perspective is the ~10-cm amplitude transient displacements computed from the downhole accelerogram. These transient displacements beneath the liquefied layer suggest that long-period ground motion continued to shake the array after strong motion abated.

To better understand the nature of these displacements, Figure 10 shows the time histories of displacements computed from all three components of the downhole accelerograms as well as particle motion in map view. As can be seen in Figure 10a, most of the motion is occurring in the horizontal plane with a periodicity of ~5.5 sec. Vertical displacements are small (<2 cm) relative to the horizontal displacements. When examined in map view (Fig. 10b), the particle motion is essentially polarized in a northwest–southeast direction, which also approximately parallels the Superstition Hills fault (Fig. 1). These observations indicate that Wildlife was continuing to be seismically excited by

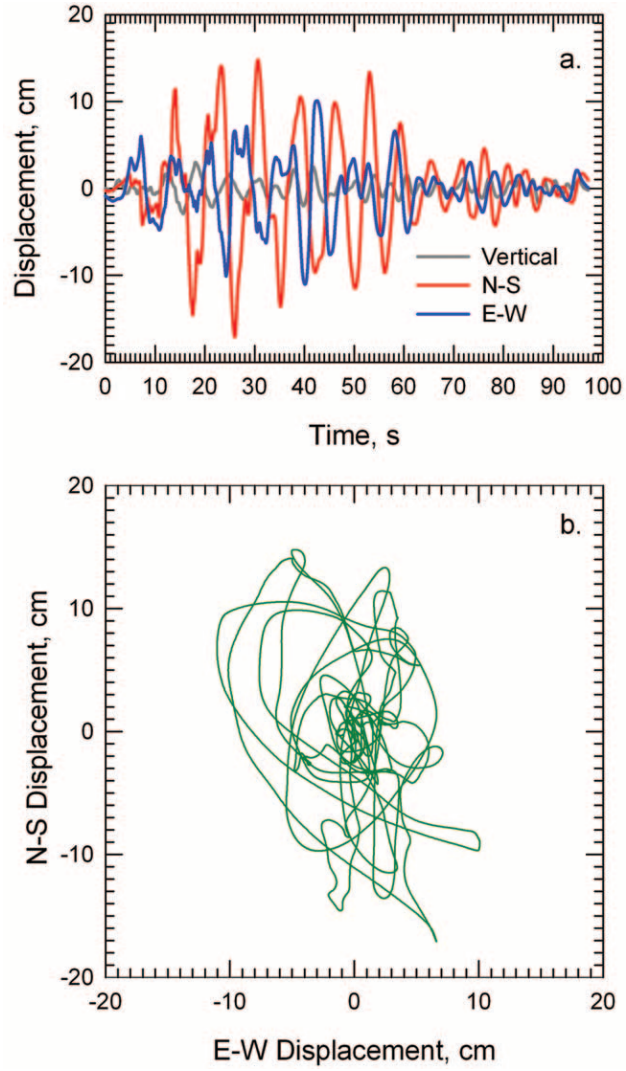

Figure 10. Displacements computed from downhole accelerograms: (a) time histories of vertical, north–south and east–west components of displacement; (b) horizontal particle motion.

5.5-sec-period Love waves during the 97-sec-long record. The amplitude of the acceleration was greater than 0.01*g*, which qualifies the shaking as strong motion to seismologists (Anderson, 2003), although this level of shaking, in general, is not considered to be of engineering significance. We will argue in the Discussion that this motion caused the delayed buildup of excess pore-water pressure.

Permanent Deformation

On 8 April 1988, 135 days after the earthquake, an inclinometer casing that had been installed before the earthquake to a depth of ~8.6 m was resurveyed (Table 2). The casing consisted of aluminum tubing with a 70.9-mm outside diameter and 2.0-mm wall thickness. It was installed in three 3-m-long sections and no measures were taken to assure that the casing was installed vertically. The top two panels of

Table 2
Cumulative Deflection from Vertical of Inclinometer Casing Relative to Base of Casing as Measured on 8 April 1988

	Cumulative Deflection (mm)	
Depth (m)	N20°W	N70°E
0.1	147.9	102.8
0.6	145.9	97.1
1.1	143.5	91.5
1.6	139.7	86.3
2.1	132.5	80.3
2.6	118.9	71.7
3.1	100.4	62.6
3.6	81.1	53.6
4.1	61.5	45.9
4.6	44.0	39.7
5.1	30.3	34.0
5.6	20.1	28.8
6.1	12.9	23.7
6.6	8.1	18.9
7.1	4.9	13.9
7.6	2.5	8.9
8.1	1.0	4.5
8.6	0	0

Figure 11 shows orthogonal profiles of the casing after the earthquake. The bearing of each profile is shown in the upper right corner of the panel. If the casing is assumed to have been originally straight and vertical, the resultant deflection from the vertical implies that the ground moved 180 mm in a N15°E direction (Fig. 11c). Assuming an originally straight vertical casing, the tilt of the casing indicates the permanent shear strain. The resulting estimated shear-strain profiles are consistent with each other and suggest that the shearing associated with lateral spreading at Wildlife was primarily in the upper portion of the liquefied layer. The maximum shear strain as computed from the resultant of the two components is 4.3% in a N15°E direction (Fig. 11c).

Unfortunately, the pre-earthquake survey of the casing was lost so that the original shape and orientation of the casing are undocumented. Nevertheless, plots of cumulative deflection of the casing relative to its base and the implied shear strain in Figure 11 allow us to distinguish approximately between real deformation and artifacts of the original shape and orientation of the casing. The large, but approximately uniform, N70°E shear strain, ~1%, is suspicious and suggests the inclinometer casing originally was straight but tilted 1% in the N70°E direction. In other words, if the casing were indeed originally straight but tilted, the assumption of verticality would produce a uniform shear strain like that which is computed in the top and bottom of the casing. If this uniform strain is subtracted from the total strain, the casing was deflected only approximately 20 mm by the lateral spreading. The remaining 83 mm of the 103 mm of measured deflection by this interpretation is a relic of original tilt of the casing. By similar reasoning, 20 mm of the 148-mm deflection in the N20°W direction is a relic of the original tilt of the casing. Thus, if the casing is assumed to

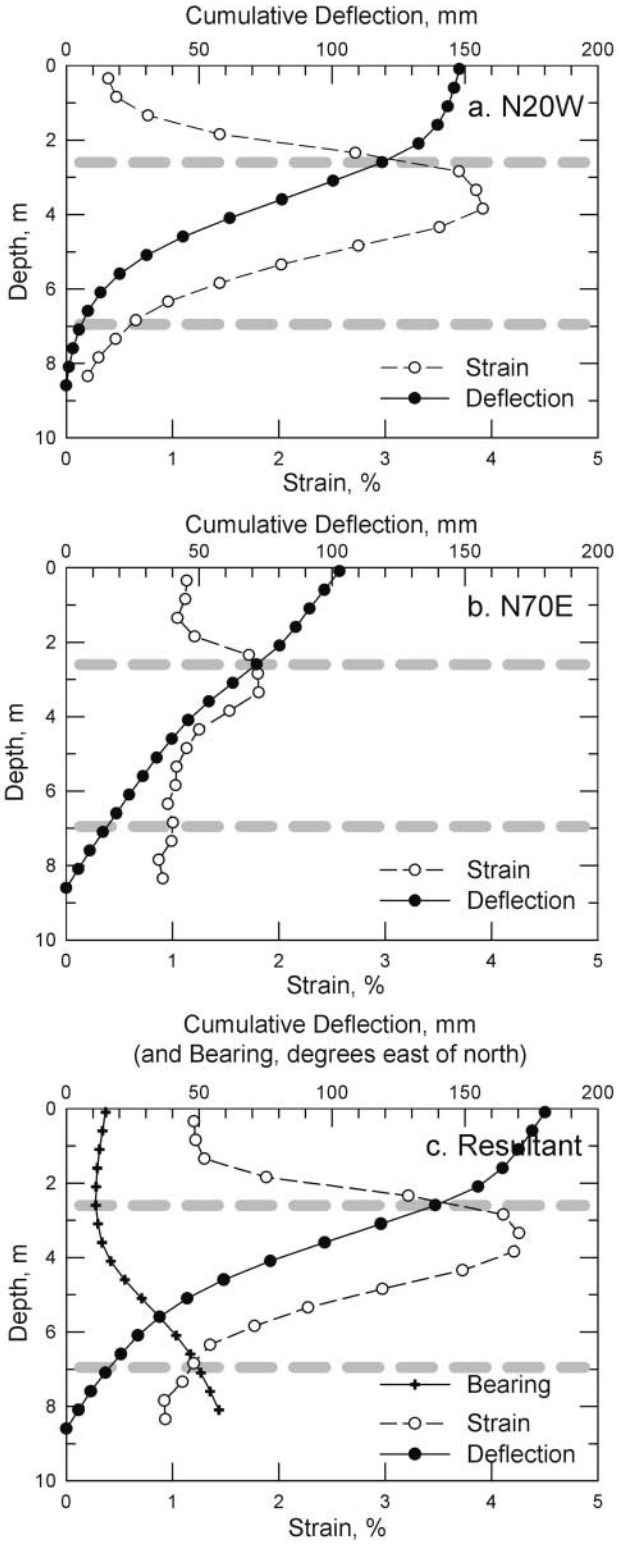

Figure 11. Deflection of inclinometer casing from vertical and computed shear strain. Panels a and b are orthogonal components and panel c is the resultant. Thick dashed horizontal lines are the upper and lower boundaries of liquefiable layer inferred from nearby CPT soundings; thickness of line reflects uncertainty of depth estimates.

have been originally straight but tilted the aforementioned amounts, the resultant ground displacement is 130 mm in a N10°W direction and the associated maximum shear strain is approximately 3%.

Either interpretation leads to the same general conclusion concerning the deformation of the sand layer at the Wildlife site. The ground moved between 130 and 180 mm in a northerly direction, and most of the permanent shear strain occurred in the upper part of the liquefied sand layer. We note, however, that both interpretations of displacement inferred from the inclinometer casing are slightly larger than the displacement, 107 mm, measured at the nearby control points (Fig. 3). In addition, only the first interpretation produces a displacement parallel to that predicted by the control points. Both sets of measurements, however, imply northerly ground displacement of ~100 mm.

The northward permanent ground displacement determined from the survey of the inclinometer and control points may explain why the largest pore-water pressure drops occurred when the ground was oscillating northward. As noted by Zegahl and Elgamal (1994), the asymmetry of the hysteresis loops and greater dilatancy in the northern (positive strain) direction (see Figs. 8 and 9) most likely was caused by bias in the static shear stress that caused the lateral spread to move in a northerly direction. This explanation is illustrated in Figure 12. In Figure 12, an arbitrary time-dependent and northward permanent displacement of 100 mm associated with the lateral spreading was added to the transient north–south surface displacements shown in Figure 6. We assumed that the northward component of lateral spreading started at 18.7 sec (when the first pore-water pressure drop was recorded by P5) and occurred at a constant rate until 90 sec (when shaking and pore-water pressure buildup were essentially complete). The difference between the estimated surface displacement and displacement computed from the

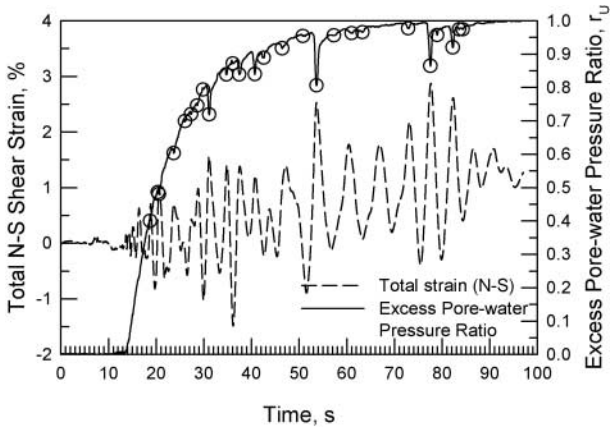

Figure 12. Time histories of estimated north–south total shear strain and excess pore-water pressure ratio recorded by P5. Total shear strain is the sum of the transient strains and an assumed permanent strain history of the lateral spread. Drops of pore-water pressure are circled.

downhole accelerometer when divided by 7.5 m is the average total (transient plus permanent) shear strain to a depth of 7.5 m. Whereas the amount of lateral spreading displacement and its time history are arbitrary, the time history plotted in Figure 12 shows the general pattern of the time history of the total shear strain.

Effect on Penetration Resistance

To determine the potential impact of liquefaction on penetration resistance in the sand layer, nine CPT soundings were conducted 4½ months after the earthquake next to three soundings that were conducted in 1982 at the time that the array was established. Three soundings were conducted within 1 m of each of the 1982 soundings in a triangular pattern. Both the original and postearthquake soundings were conducted with the same CPT cone, which was calibrated before each field campaign. Original and postearthquake CPT profiles are shown in Figure 13a. Locations of the three original soundings, 3Cg, 5Cg, and 6Cg, are shown in Figure 3. The only consistent trend when the average postearthquake profile is compared with the pre-earthquake CPT profile is that the sleeve friction is generally higher by 30 to 40 kPa at all three locations in most of the liquefiable layer (Fig. 13a). The difference in sleeve friction between post- and pre-earthquake profiles is typically more than 50% (Fig. 13b). The difference between post- and pre-earthquake tip resistance is not consistent within the layer. Both higher and lower tip resistances were measured after the earthquake relative to pre-earthquake values (Fig. 13b). Douglas and Olsen (1981) indicate an increase of K_0, the coefficient of earth pressure at rest, would have a larger effect on sleeve resistance than on tip resistance. Thus, we tentatively attribute the increase of sleeve friction to an increase of horizontal stress. A striking aspect of each set of three postearthquake CPT profiles, however, is the large natural lateral variability of the liquefiable layer over distances of only 1 m (Fig. 13a). This large natural variability makes detection of earthquake-induced changes challenging.

About 10 hours after the earthquake, the first author visited the site and estimated the total volume of water and sediment that discharged to the ground surface by surveying the pool of water and sediment that was retained in a closed basin at the site. The average depth of water and thickness of ejecta was no more than 50 mm. This thickness was approximately 1% of the total thickness of the sand layer and indicates that the average volumetric strain within the layer was approximately 1%.

Based on the reduction in volume of the sand layer, it is instructive to estimate the impact of the associated increase in relative density on tip resistance. To make this estimate, we used the relation between tip resistance and relative density proposed by Kulhawy and Mayne (Lunne *et al.*, 1997, p. 84), in which normalized cone resistance is proportional to the square of relative density. For demonstration, we will assume that most of the ~1% volume change was caused by expulsion of water and therefore is a reduction in pore volume. We also assume a homogeneous sand layer. If a pre-earthquake relative density of the liquefied silty sand at Wildlife of 30% is assumed, a 1% volume change implies that relative density increased to 32.1%. This assumes a maximum and minimum void ratio of 0.9 and 0.3, respectively, for the silty sand (Lambe and Whitman, 1969, p. 31). According to Kulhawy and Mayne, this increase of relative density implies an increase of tip resistance of approximately 14%. Similarly, if the original relative density equaled 40% (25%), tip resistance would increase 12% (18%). These estimated increases of tip resistance are difficult to discern with only a few soundings when confronted with the natural large lateral variability at Wildlife.

Discussion

The challenge to understanding the Wildlife recordings was summarized succinctly by Scott and Hushmand (1995) in their discussion of Youd and Holzer (1994). They pointed out that the buildup of pore-water pressure did not conform to expectations. Such an outcome raises the question whether the observed pore-water pressure behavior was the result of faulty piezometers rather than a natural phenomenon. Hushmand *et al.* (1992, p. 1266) argued that "No mechanism is known by which a soil element could be subjected to a rapid shearing strain, and respond with a delayed pore pressure rise." We are now prepared to argue that the slow pore-water pressure buildup was not delayed, but caused by ongoing cyclic shear strains associated with long-period Love waves. We also will show that the buildup is consistent with fundamental principles of the liquefaction process (National Research Council, 1985).

Before we argue that all of the piezometers recorded a natural phenomenon, we review for the reader's benefit what is known about their response. First, all the functioning piezometers in the liquefied layer in 1987 recorded the delay in the buildup of pore-water pressure to approximately static effective overburden stress (Figs. 14a and b). The buildup began simultaneously at 13.6 sec at each of the piezometers. Figure 14a shows the absolute excess pore-water pressures recorded by all of the piezometers; these recordings are not corrected for drift. Excess pore-water pressure at each piezometer ultimately attained the approximate static effective overburden stress, which is labeled on each recording in Figure 14a. We assume that the discrepancies between measured and estimated values are primarily a result of inadequate transducer calibration and drift. Figure 14b plots the same recordings as an excess pore-water pressure ratio and corrected for drift using the same procedures that were used with P5, that is, the recording by each piezometer was corrected for drift using its Elmore Ranch earthquake recording and the excess pore-water pressure ratio was computed by dividing observed excess pore-water pressure by the value measured at 97 sec. Second, the spectral response of the piezometers varied. This is illustrated in Figure 14c, which

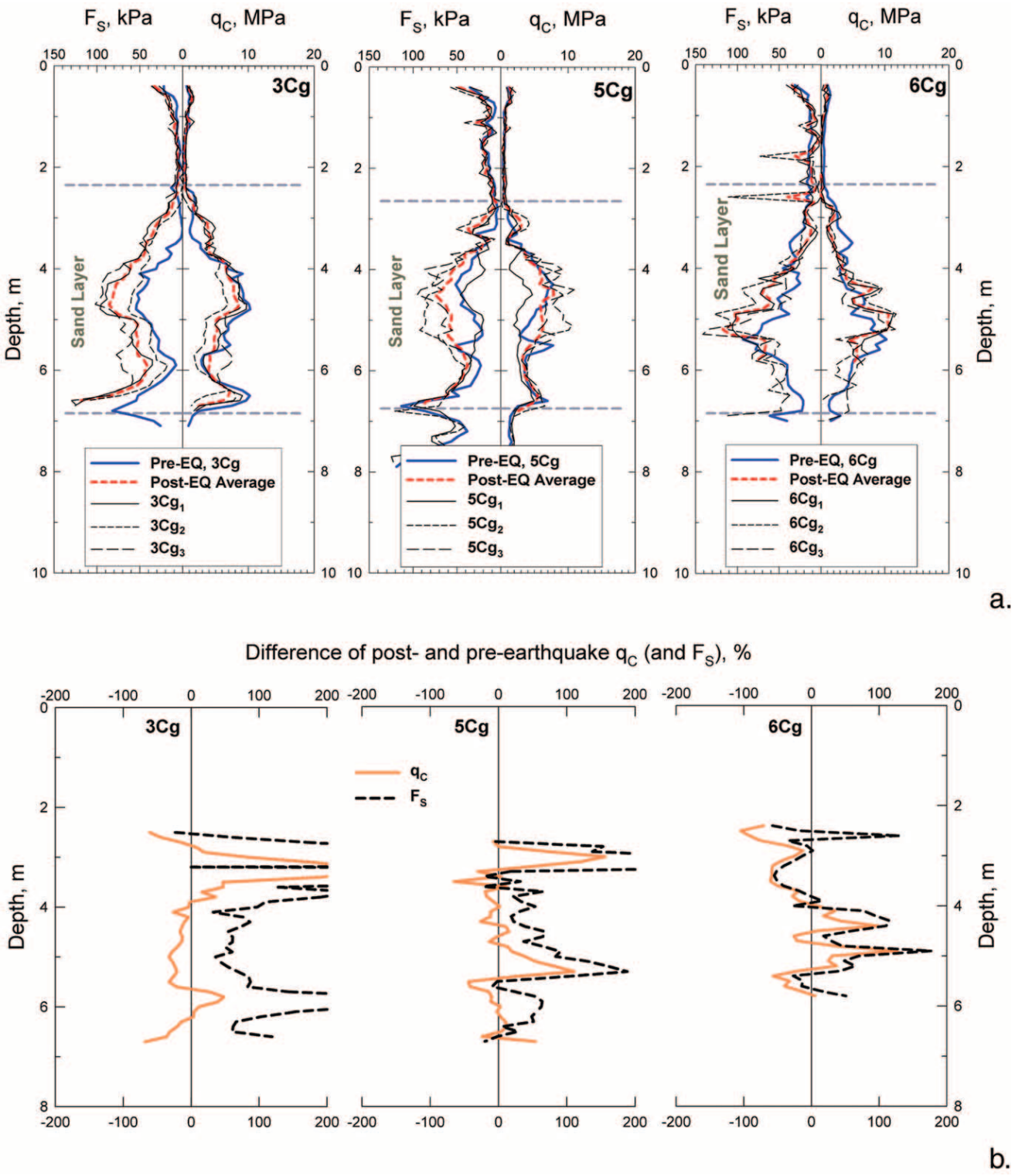

Figure 13. (a) CPT profiles at three locations conducted before and after the 1987 Superstition Hills earthquake. F_S is sleeve friction; q_C is tip resistance. Three postearthquake profiles (and their average) at each location are compared with the one pre-earthquake profile. (b) Percentage difference between average post- and pre-earthquake profiles in the liquefied sand layer.

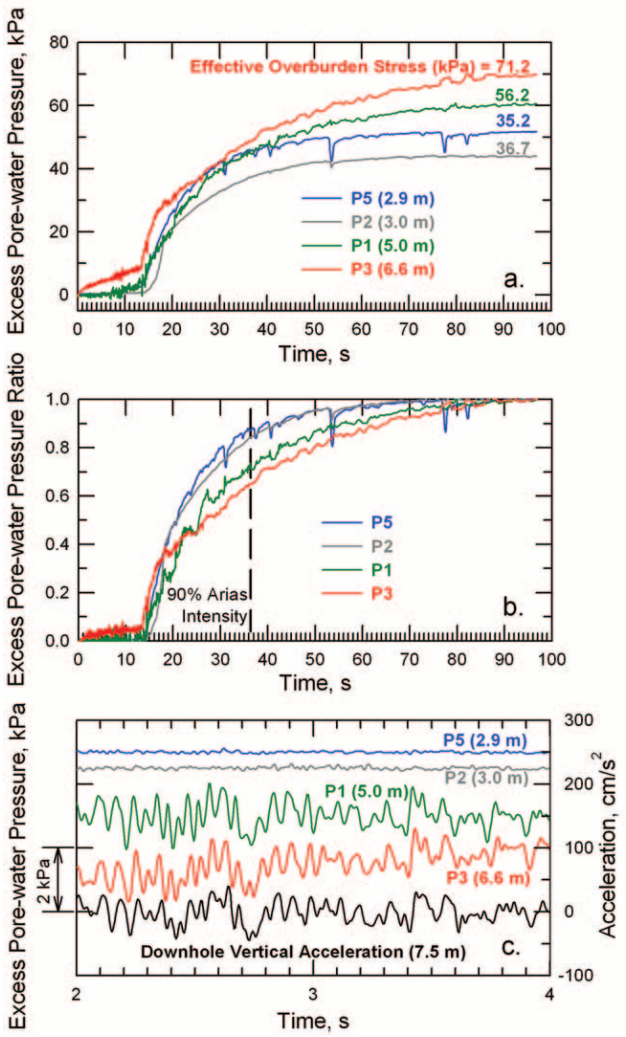

Figure 14. Pore-water pressure recordings from all piezometers in liquefied layer. (a) Excess pore-water pressures as recorded by transducers. (b) Excess pore-water pressure ratio corrected for instrumental drift. Ratio was computed by dividing by pore-water pressure recorded at 97 sec. (c) Time histories of excess pore-water pressures from 2 to 4 sec from Figure 14a (arranged by depth) and vertical acceleration recorded by downhole accelerometer.

shows the pore-water pressure time histories from 2 to 4 sec from Figure 14a. Recordings in Figure 14c are arranged by depth to avoid overlap. To improve the resolution of the recordings in Figure 14c, the original analog film record was rescanned and pore-water pressures were sampled at 200 samples per second for 2 to 4 sec. Figure 14c shows that piezometers P1 and P3 recorded high frequencies (~12 Hz), but piezometers P2 and P5, both near the top of the liquefiable layer, did not. The similar spectral responses of pore-water pressures recorded by P1 and P3 and the vertical acceleration recorded in the downhole suggest that these piezometers are responding to volumetric strains associated with *P* waves generated by the earthquake. Piezometers P2 and P5, which do not seem to be excited by the *P* waves, do respond, however, at slightly lower frequencies as indicated by the 0.5- to 1-Hz pore-pressure drops that occur later in the recordings (Fig. 14a).

The assumption that excess pore-water pressures approximately reached the static effective overburden stress is particularly relevant to results from the *in situ* evaluation of the piezometers by Earth Technology Corporation (1991) that formed the basis for the challenge by Scott and Hushmand (1995). The tests, conducted 2 years after the Superstition Hills earthquake, subjected the transducers to low-frequency (0.2-Hz) pulsating pressure tests, pressure surges, and a dead-weight drop. Piezometer performance was evaluated by comparison with a nearby reference transducer. The report concluded that only P5 "performed reasonably correctly." Piezometers P1 and P2 measured only a fraction of the transient ambient pore-water pressure and exhibited different decays. P3 appeared to no longer be functional. The dead-weight drop, which was recorded only by piezometers P1 and P5 and on the surface accelerometer, indicated that the P1 and P5 responded to frequencies as high as 20 to 30 Hz.

Building on the work by Zegahl and Elgamal (1994), who were the first to demonstrate that transient shear strains in the liquefying layer continued after the strong motion had abated, we now explain the physical origin of these strains and demonstrate that the recorded pore-water pressure buildups are consistent with our understanding of the liquefaction process, Scott and Hushmand's (1995) challenge not withstanding. Figures 6 and 10 show that the transient shear strains were caused by ~10-cm-amplitude, 5.5-sec-period Love waves that continued to strain the soil well after strong shaking had abated. Seed and Lee (1966) in their laboratory investigation showed that subjecting sand to cyclic loads of constant strain amplitude leads to a progressive buildup of pore-water pressure as the number of strain cycles increases (Fig. 15). The buildup causes strain softening and ultimately liquefaction, if the duration is sufficient. In a prescient description that could be applied to Wildlife, they note "the hysteresis curves of stress versus strain become progressively flatter, ultimately becoming horizontal when the soil liquefies" (Seed and Lee, 1966, p. 122). This behavior is consistent with dynamic densification of sand, which is actually controlled by the amplitude of cyclic strain, not the magnitude of cyclic stress (Silver and Seed, 1971; Youd, 1972). Comparison of the Wildlife recordings (Fig. 7) with Seed and Lee's (1966) empirical observation of liquefaction by constant-amplitude cyclic strains (Fig. 15) is compelling and implies the same phenomenon is occurring in both situations.

Not only is the buildup of pore-water pressure recorded by each piezometer consistent with Seed and Lee's (1966) strain mechanism, but the depth sequence in which the layer liquefied is consistent with the prediction by Seed and Lee (1966, p. 131–132) that liquefaction of a deposit will propagate sequentially downward. At Wildlife, pore-water pres-

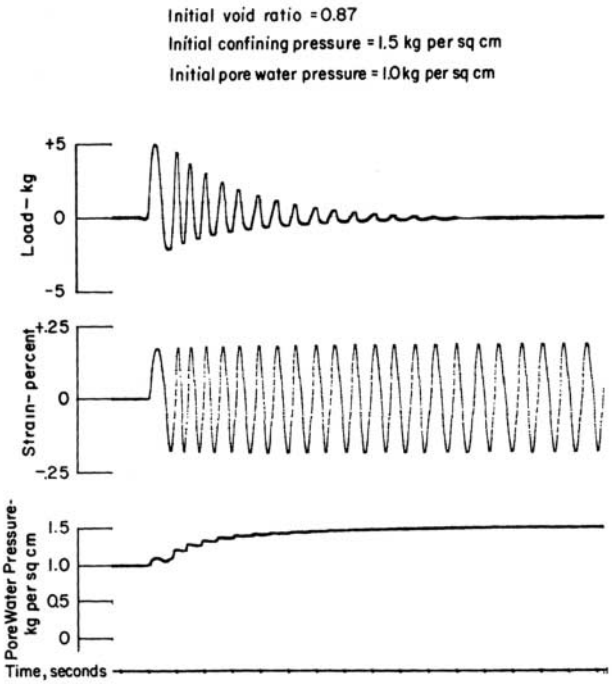

Figure 15. Constant-amplitude cyclic strain test on Sacramento River sand (Seed and Lee, 1966, Fig. 12).

sure first equaled effective overburden stress in the upper part of the layer and then progressively reached the effective overburden stress in a downward direction (Fig. 14b). This progression also implies that the proportional contribution of the Love waves to total excess pore-water pressure increased with depth. Although it is difficult to isolate precisely the amount to which Love waves contributed to pore-water pressure generation, Figures 4 and 5 indicate that high-frequency strong ground motion had diminished at 36.4 sec when 90% of the Arias Intensity had accumulated. If this time is used to approximate the cessation of excitation by body waves, Love waves caused 13, 16, 28, and 35%, respectively, of the excess pore-water pressure, buildup at piezometers P5 (2.9 m), P2 (3.0 m), P1 (5.0 m), and P3 (6.6 m) (Fig. 14b).

This conclusion has important implications for understanding liquefaction under field conditions. Perhaps, foremost of these is recognition of the potential for long-period but large-amplitude cyclic displacements to be significant generators of excess pore-water pressure. Although it is clear from Figure 6 that the initial buildup of excess pore-water pressure was caused by strains associated with high-frequency strong ground motion, it appears that Wildlife would not have liquefied if this ground motion had not been followed by the weaker long-period oscillatory motion associated with the Love waves. Pore-water pressures would have reached only 65 to 87% of the overburden stress, depending on depth and assuming no pore-water pressure migration. Because long-period surface waves are to be expected in the geologic setting of many liquefaction sites, which commonly are in deep sedimentary basins, the observations at Wildlife may be more typical than atypical.

It is useful to speculate why pore-pressure drops were largest in the shallow piezometer, P5. The drops themselves are not surprising and are consistent with laboratory experiments involving shearing of sands. As a soil decreases in volume when cyclically strained, "each half cycle causes some expansion (dilation) of the sand as particles are forced to roll or slide up on adjacent particles" (National Research Council, 1985, p. 37). Such dilation under undrained loading will be manifested as a pore-pressure drop. As was discussed in the section *Permanent Deformation*, the large drops observed in P5 coincide with northern transient strains. As noted by Zegahl and Elgamal (1994), the large drops could be caused by bias in the static shear stress associated with the free face of the river. The concentration of permanent shear strain as recorded by the inclinometer casing in the upper part of the liquefied layer is consistent with a biasing static shear stress in that part of the layer.

Although more speculative, the Wildlife recordings may provide insight into the mechanism of lateral spreading. The asymmetry of the hysteresis curves with the greater dilatancy in the northern direction as evidenced by the pore-water pressure drops suggests that lateral spreading was occurring during the latter 80 sec of the Wildlife recordings. If this interpretation is valid, it appears that the ground moved in a series of lurches caused by the cyclic straining associated with the long-period Love waves. We speculate that the time history in Figure 12 approximately describes the movement of the lateral spread.

Finally, we propose that the long-period Love waves (and possibly Raleigh waves at other sites) are the cause of ground oscillation that has been reported by some observers (National Research Council, 1985). By this mechanism, the reported jostling of blocks back and forth is caused by the underlying soil cycling back and forth as long-period surface waves propagate through a liquefying site. We interpret the surface displacement shown in Figure 6 as ground oscillation.

Implications for Engineering Practice

The Wildlife recordings expose at least two epistemological shortcomings in the widely used Seed–Idriss simplified procedure and efforts to expand it into a probabilistic framework (e.g., Cetin *et al.*, 2004; Moss, *et al.*, 2006). First, recognition that long-period surface waves can generate significant excess pore-water pressure highlights an inherent limitation in the stress-based characterization of seismic demand used in the procedure. Whereas it has been acknowledged for many years that densification of sand is controlled by the amplitude of cyclic strain, the average cyclic shear stress, which is computed from PGA, is used in the simplified procedure for practical convenience. The contribution of long-period cyclic shear strains at Wildlife to achieving a

zero effective stress condition suggests that computing seismic demand with a strain parameter is more realistic. Such a strain-based approach was proposed by Dobry *et al.* (1982). Second, the contribution to pore-water pressure buildup from large cyclic strains at small ground accelerations (and cyclic stress levels) is relevant to magnitude-scaling factors, which are used in the simplified procedure to estimate the number of equivalent uniform stress cycles. These factors assume that earthquake magnitude is a reliable predictor of the number of cycles. The Wildlife records indicate that as the sand softens during the liquefaction process, low cyclic stress levels associated with surface waves can be significant generators of excess pore-water pressure. Because the amplitude of surface waves depends strongly on basin velocity structure, the seismic demand imposed at two different sites may be very different for earthquakes of the same magnitude, level of cyclic stressing, and number of stress cycles. Thus, when magnitude-scaling factors are used to convert earthquakes to a reference magnitude (usually M 7.5) in the simplified procedure, actual seismic demands of the earthquakes may differ even when the number of stress cycles are correctly computed. It is unclear to us how these strain-based considerations can be reconciled with a stress-based methodology. Thus, the Wildlife recordings indicate that reliance on a stress-based methodology may introduce significant epistemic uncertainty into probabilistic formulations of the simplified procedure.

Recognition that ground oscillation is the manifestation of Love waves propagating through a liquefied site improves the capability to predict locations where buried lifelines may be at greater risk. As pointed out by Pease and O'Rourke (1997), ground oscillation can cause large and damaging differential ground strains where liquefied layers are laterally bounded by competent soils. Because long wave trains of large-amplitude surface waves typically are generated in sedimentary basins, ground oscillation that may damage buried lifelines is more likely in such geologic settings. This damaging process could also apply to surface structures such as bridges that span these boundaries.

Generation of pore-water pressure by Love waves may also explain why some liquefaction effects are delayed after earthquakes. Typically these delayed effects are attributed to pore-pressure migration or slow dissipation of excess pore-water pressure. A possible example is the failure of the Showa Bridge in the 1964 Niigata, Japan, earthquake. Eyewitness reports of the failure of the bridge indicated the spans of the bridge collapsed into the Shinanogawa River perhaps as much as one minute after strong shaking had ended (Horii, 1968, p. 438–448; Hamada, 1992, p. 3-25–3-28). Hamada (1992, p. 3-27) also reported an "eyewitness on one bank said that damage to the revetment on the left bank of Showa Bridge began after the earthquake." Our interpretation of the Wildlife recordings suggests the delayed collapse of the bridge may have been caused by continued generation of pore-water pressure by long-period surface waves. Double integration by Carter (2004) of the accelerogram recorded in Kawagishi-cho revealed that long-period cyclic displacements with amplitudes of 10 to 25 cm continued for at least 100 sec after the accelerograph triggered. This long-period ground motion suggests that cyclic straining and pore-pressure generation within the 7- to 8-m-thick liquefiable sand layer by surface waves like those that caused liquefaction at Wildlife may have continued after the stronger ground shaking abated.

Finally, the inability to detect significant changes in CPT tip resistance caused by liquefaction in 1987 is consistent with the practice of using postearthquake penetration resistance to predict liquefaction potential with the Seed–Idriss simplified procedure (Youd *et al.*, 2001). The liquefaction case histories on which the procedure is based rely on post-earthquake penetration resistance measurements. The impact of using either pre- or postearthquake soundings to compute factors of safety for the Superstition Hills earthquake is illustrated in Figure 16. Factors of safety for the postearthquake condition in each panel are based on the average of penetration resistance of the three CPT soundings that were adjacent to the single pre-earthquake sounding. Both pre- and postearthquake soundings predict liquefaction in the sand layer during the Superstition Hills earthquake. Factors of safety for the Elmore Ranch earthquake computed with only the pre-earthquake CPT sounding are also shown and do not predict liquefaction for that event. The slightly lower factors of safety computed for the mainshock when using the pre-earthquake soundings are the result of the Robertson and Wride (1997) methodology that we used. It relies on friction ratio to make a correction for soil type. If we had used an alternative CPT-based method that relied only on tip resistance and direct measurements of grain size and soil type, factors of safety based on post- and pre-earthquake soundings would be even more similar.

Published comparisons of post- to pre-earthquake penetration tests from other earthquakes are inconsistent on this issue. Comparisons of standard penetration test (SPT) blow counts after the 1964 Niigata, Japan, earthquake, with pre-earthquake tests indicated that some profiles of penetration resistance showed increases of blow counts in the top and decreases in the bottom portions of the liquefied interval (and vice versa). Other profiles indicated an overall decrease (Hayashi *et al.*, 1966). They attributed the decreases of penetration resistance to dilation associated with shearing. Chameau *et al.* (1991) compared adjacent post- with pre-earthquake CPT profiles in sandy artificial fills that were shaken by the 1989 Loma Prieta, California, earthquake, and observed increases of tip resistance in loose- to medium-dense sands, but not in denser sands. Their observations are consistent with those of Seed *et al.* (1988) who analyzed the change in density of the medium-dense hydraulic fill in Lower San Fernando Dam that liquefied during the 1971 San Fernando earthquake. They reported that SPT blow counts were larger after the earthquake.

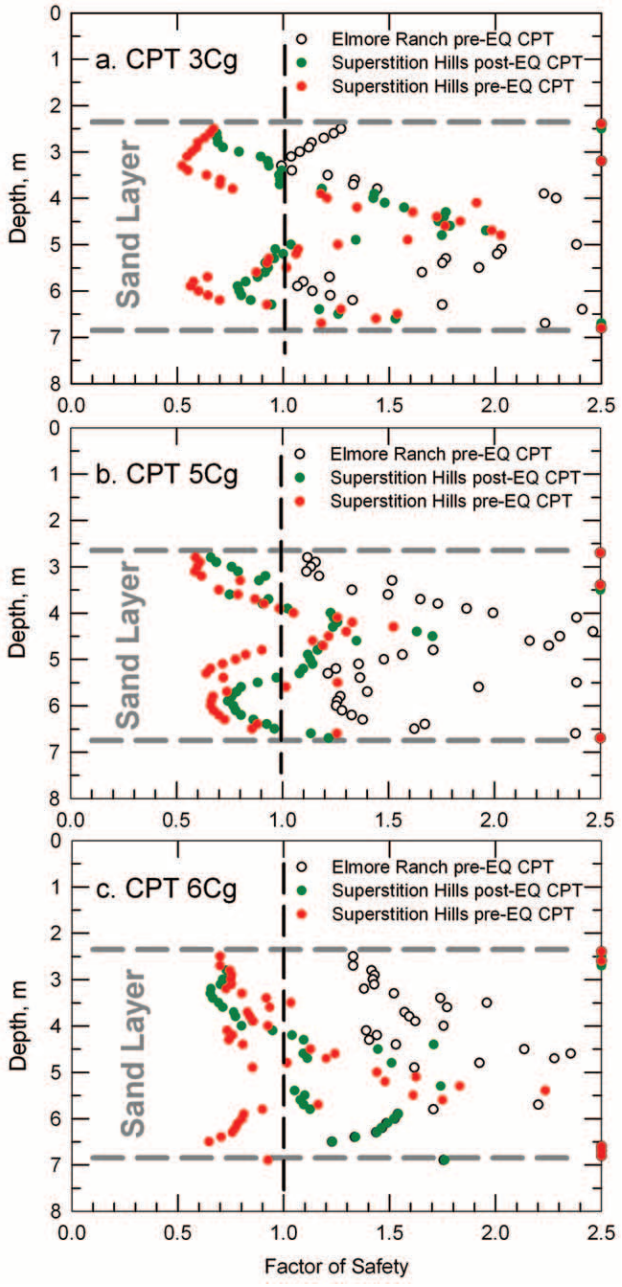

Figure 16. Factors of safety in liquefied sand layer computed with (1) pre- and average of three postearthquake CPT soundings for the Superstition Hills earthquake and (2) with pre-earthquake CPT soundings for the Elmore Ranch earthquake.

Acknowledgments

We greatly appreciate discussions and help from several colleagues. We especially want to acknowledge discussions with Ross W. Boulanger that clarified the implications of the hysteresis curves. Christopher D. Stephens was exceptionally helpful with the record processing and clarified many filtering issues. David M. Boore shared his insight into the seismology of the Wildlife records. Michael J. Bennett prepared Table 1. Robert L. Nigbor suggested comparing high-frequency pore-water pressure fluctuations with the vertical accelerations. Pedro A. de Alba and Jamison H. Steidl provided constructive reviews of drafts of the manuscript. Finally, we thank the anonymous Bulletin reviewers for their suggestions.

References

Anderson, J. G. (2003). Strong-motion seismology, in *International Handbook of Earthquake and Engineering Seismology: Part B*, W. H. K. Lee, H. Kanamori, P. C. Jennings, and C. Kisslinger (Editors), Academic Press, Amsterdam, 937–965.

Arias, A. (1969). A measure of earthquake intensity, in *Seismic Design for Nuclear Power Plants*, R. Hansen (Editor), MIT Press, Cambridge, Massachusetts, 439–483.

Bennett, M. J. (1988). Sand boils and their source beds-November 24, 1987, Superstition Hills earthquake, Imperial Valley, California (abstract), *Assoc. Eng. Geol. Abstracts Program* **31,** 38.

Bennett, M. J., P. V. McLaughlin, J. S. Sarmiento, and T. L. Youd (1984). Geotechnical investigation of liquefaction sites, Imperial Valley, California, *U.S. Geol. Surv. Open-File Rept. 84-252*, 103 pp.

Bierschwale, J. G. (1984). Analytical evaluation of liquefaction potential of sands subjected to the 1981 Westmorland earthquake, University of Texas, Civil Engineering Department Geotechnical Engineering Report GR-84-15, 231 pp.

Bonilla, L. F., R. J. Archuleta, and D. Lavallée (2005). Hysteretic and dilatant behavior of cohesionless soils and their effects on nonlinear site response: field data observations and modeling, *Bull. Seism. Soc. Am.* **95,** 2373–2395.

Carter, B. L. (2004). Influence of soil softening and liquefaction on response spectra, M.S. Thesis, Brigham Young University Department of Civil and Environmental Engineering, 195 pp.

Cetin, K. O., R. B. Seed, A. D. Kiureghian, K. Tokimatsu, L. F. Harder, R. E. Kayen, and R. E. S. Moss (2004). Standard penetration test-based probabilistic and deterministic assessment of seismic soil liquefaction potential, *J. Geotech. Geoenviron. Eng. ASCE* **130,** 1314–1340.

Chameau, J. L., G. W. Clough, F. Reyna, and J. D. Frost (1991). Liquefaction response of San Francisco bayshore fills, *Bull. Seism. Soc. Am.* **81,** 1998–2018.

Davis, R. O., and J. B. Berrill (2000). Wildlife revisited, in *John Booker Memorial Symposium*, D. W. Smith and J. P. Carter (Editors), Balkema, Rotterdam, The Netherlands, 355–370.

Dobry, R., R. S. Ladd, F. Y. Yokel, R. M. Chung, and D. Powell (1982). *Prediction of pore water Pressure Buildup and Liquefaction of Sands during Earthquakes by the Cyclic Strain Method, NBS Building Science Series 138*, National Bureau of Standards, Gaithersburg, Maryland, 150 pp.

Douglas, B. J., and R. S. Olsen (1981). Soil classification using electric cone penetrometer, in *Proc. Conf. On Cone Penetration Testing and Experience*, G. M. Norris and R. D. Holtz (Editors), *ASCE* Geotechnical Engineering Division, St. Louis, 26–30 October, 209–227.

Earth Technology Corporation (1991). Final report, Accuracy of the pore-water pressures recoded at Wildlife site during magnitude 6.6 Imperial Valley earthquake of 24 November 1987, Unpublished Rept. to U.S. Geol. Surv., Reston, Virginia, 62 pp.

Glaser, S. (1996). Insight into liquefaction by system identification, *Géotechnique* **46,** 641–655.

Gu, W. H., N. R. Morgenstern, and P. K. Robertson (1994). Postearthquake deformation analysis of the Wildlife site, *J. Geotech. Eng. ASCE* **120,** 274–289.

Hamada, M. (1992). Large ground deformations and their effects on lifelines: 1964 Niigata earthquake, in *Case Studies of Liquefaction and Lifeline Performance during Past Earthquakes*, M. Hamada, M. Hamada, and T. D. O'Rourke (Editors), National Center for Earthquake Engineering Tech. Rept. NCEER-92-001, 3-1–3-123.

Hayashi, S., K. Kubo, and A. Nakase (1966). Damage to harbour structures by the Niigata earthquake, *Soils Found.* **6,** 89–112.

Holzer, T. L., T. L. Youd, and M. J. Bennett (1989a). In situ measurement of pore pressure buildup during liquefaction, in *Proc. 20th Joint Meeting of the U.S.-Japan Cooperative Program in Natural Resources, Panel on Wind and Seismic Effects*, National Institute of Standards and Technology Special Paper 760, 118–130.

Holzer, T. L., T. L. Youd, and T. C. Hanks (1989b). Dynamics of liquefaction during the 1987 Superstition Hills, California, earthquake, *Science* **244,** 56–59.

Horii, K. (1968). Highway bridges, in *General Report on the Niigata Earthquake of 1964*, H. Kawasumi (Editor), Tokyo Electrical Engineering College Press, 438–448.

Hushmand, B., R. F. Scott, and C. B. Crouse (1991) In-situ calibration of USGS piezometer installations, in *Recent Advances in Instrumentation, Data Acquisition, and Testing in Soil Dynamics*, S. K. Bhatia and G. W. Blaney (Editors), ASCE Special Publication 29, 49–61.

Hushmand, B., R. F. Scott, and C. B. Crouse (1992). In-place calibration of USGS pore pressure transducers at Wildlife Liquefaction Site, California, USA, in *Proc. 10th Earthquake Engineering World Conference*, Balkema, Rotterdam, The Netherlands, 1263–1268.

Lambe, T. W., and R. V. Whitman (1969). *Soil Mechanics*, John Wiley and Sons, New York, 553 pp.

Lunne, T., P. K. Robertson, and J. J. M. Powell (1997). *Cone Penetration Testing in Geotechnical Practice*, Spon Press, London, 312 pp.

Moss, R. E. S., R. B. Seed, R. E. Kayen, J. P. Stewart, A. D. Kiureghian, and K. O. Cetin (2006). CPT-based probabilistic and deterministic of in situ seismic liquefaction potential, *J. Geotech. Geoenviron. Eng. ASCE* **132,** 1032–1051.

National Research Council (1985). *Liquefaction of Soils during Earthquakes*, Committee on Earthquake Engineering, National Academy of Sciences, Washington, D.C., 240 pp.

Pease, J. W., and T. D. O'Rourke (1997). Seismic response of liquefaction sites, *J. Geotech. Eng. ASCE* **123,** 37–45.

Robertson, P. K., and C. E. Wride (1997). Cyclic liquefaction and its evaluation based on the SPT and CPT, in *Proceedings of the NCEER Workshop on Evaluation of Liquefaction Resistance of Soils*, T. L. Youd and I. M. Idriss, (Editors), National Center for Earthquake Engineering Tech. Rept. NCEER-97-0022, 41–87.

Scott, R. F., and B. Hushmand (1995). Discussion of "Piezometer at Wildlife liquefaction site" by T. L. Youd and T. L. Holzer, *J. Geotech. Eng. ASCE* **121,** 912–919.

Seed, H. B., and K. L. Lee (1966). Liquefaction of saturated sands during cyclic loading, *J. Soil Mech. Found. Eng. ASCE* **92,** 105–134.

Seed, H. B., R. B. Seed, L. F. Harder, and H-L. Jong (1988). Re-evaluation of the slide in the Lower San Fernando Dam in the earthquake of Feb. 9, 1971, University of California Earthquake Engineering Research Center, Rept. no. UCB/EERC-88/04, 118 pp.

Silver, M. L., and H. B. Seed (1971). Volume changes in sands during cyclic loads, *J. Soil Mech. Found. Eng. ASCE* **97,** 1171–1182.

Vucetic, M., and R. Dobry (1986). Pore pressure build-up and liquefaction at level sandy sites during earthquakes, Rensselaer Polytechnic Institute Res. Rept. CE-86-3.

Youd, T. L. (1972). Compaction of sands by repeated straining, *J. Soil Mech. Found. Eng. ASCE* **98,** 709–725.

Youd, T. L., and S. F. Bartlett (1989). U.S. case histories of liquefaction-induced ground displacement, in *Proc. of the 2nd U.S.-Japan Workshop on Liquefaction, Large Ground-Deformation* and Their Effects on Lifelines, National Center for Earthquake Engineering Tech. Rept. NCEER-89-0032, 22–31.

Youd, T. L., and B. L. Carter (2005). Influence of soil softening and liquefaction on spectral acceleration, *J. Geotech. Geoenviron. Eng. ASCE* **131,** 811–825.

Youd, T. L., and T. L. Holzer (1994). Piezometer performance at Wildlife liquefaction site, California, *J. Geotech. Eng. ASCE* **120,** 975–995.

Youd, T. L., and G. F. Wieczorek (1982). Liquefaction and secondary ground failure, in *The Imperial Valley, California, Earthquake of October 15, 1979, U.S. Geol. Surv. Profess. Pap. 1254*, 223–246.

Youd, T. L., I. M. Idriss, R. D. Andrus, I. Arango, G. Castro, J. T. Christian, R. Dobry, W. D. L. Liam Finn, L. F. Harder, Jr., M. E. Hynes, K. Ishihara, J. P. Koester, S. S. C. Liao, W. F. Marcuson, III, G. R. Martin, J. K. Mitchell, Y. Moriwaki, M. S. Power, P. K. Robertson, R. B. Seed, and K. H. Stokoe, II (2001). Liquefaction resistance of soils: summary report from the 1996 NCEER and 1998 NCEER/NSF workshops on evaluation of liquefaction resistance of soils, *J. Geotech. Geoenviron. Eng. ASCE* **127,** 817–833.

Zeghal, M., and A.-W. Elgamal (1994). Analysis of site liquefaction using earthquake records, *J. Geotech. Eng. ASCE* **120,** 996–1017.

U.S. Geological Survey
345 Middlefield Road, Mail Stop 977
Menlo Park, California 94025
(T.L.H.)

Department of Civil Engineering
Brigham Young University
Provo, Utah 84602
(T.L.Y.)

Manuscript received 11 July 2006.